Remote Structural Health Monitoring of Concrete Bridge Using InSAR: A Case Study

OTHMANE LASRI[1], PIER FRANCESCO GIORDANO[1] and MARIA PINA LIMONGELLI[1,2]

ABSTRACT

Structural Health Monitoring (SHM) provides real-time information about structural damage and its evolution over time, which supports decision-makers in managing structural integrity. However, traditional SHM systems, such as vibration-based systems with accelerometers, require laborious installation and maintenance of instrumentation, including sensors, cables, and acquisition systems directly installed on the monitored structure. Recently, remote sensing through active satellites, such as new Synthetic Aperture Radar (SAR) missions, offers a promising alternative for monitoring infrastructure assets. This paper explores the use of SAR Interferometry (InSAR) processing to monitor the health of bridges. The full interferometry processing chain is based on Sentinel-1 and CosmoSKYMED synthetic aperture radar data and a combination of open-source routines from the Sentinel Application Platform (SNAP) and Stanford Method for Persistent Scatterers (StaMPS). The Permanent Scatterer Interferometry SAR (PS-InSAR) technique is used to derive displacement time histories. The applicability of this technique is evaluated on a concrete bridge located over the Oglio River in Isola Dovarese, Italy, which has GNSS receivers installed. To validate the methodology, PS-InSAR derived time histories are compared with GNSS-derived data, and both techniques are used to quantify bridge displacement rates from October 2020 to August 2022.

INTRODUCTION

In several geoscience fields, Synthetic Aperture Radar Interferometry (InSAR) is already a well-established monitoring technology [1], [2]. Recently, due to the increase in spatial and temporal resolution of Synthetic Aperture Radar (SAR) images and to the

[1]Politecnico di Milano, Milan, Italy
Department of Architecture, Built Environment and Construction Engineering. Piazza Leonardo da Vinci, 32 20133 Milan, Italy
[2]Lund Technical University, Lund, Sweden Division of Structural Engineering John Ericssons väg 1, 221 00 Lund, Sweden

devolvement of InSAR algorithms, this remote sensing technique can provide measurements also on human artifacts such as bridges [3]. The advantages of InSAR against in-situ displacement measurements obtained through inclinometers, extensometers, and GNSS receivers are several. The acquisition of InSAR data does not require in situ installations and allows for collecting data at a large scale. Another relevant aspect is that it allows for investigating the past behavior of structures by processing the images that cover the period of interest. One of the most used algorithms for InSAR is PS-InSAR (Permanent Scatterer InSAR). Despite the advantages of the PS-InSAR technology, several aspects require improvement. For instance, the accessibility of data and software remains a significant barrier for civil engineers interested in this topic. Specifically, PS-InSAR software applications are often available only through expensive licenses. The objective of this study is to assess the behavior of riverine bridges by utilizing an open-source PS-InSAR workflow based on two open-access software, namely SNAP and STAMPS [4]. Sentinel Application Platform (SNAP) is a software distributed by European Space Agency (ESA) that contains tools for generating interferograms. Two stacks of radar images are processed in this paper, provided by Sentinel 1 and Cosmo SkyMed satellite missions, respectively. The case study consists of a riverine bridge located in Isola Dovarese, a municipality of the Cremona province, Italy. A Global Navigation Satellite System (GNSS) is currently installed on the bridge to monitor displacements. The GNSS data are used to validate the PS-InSAR measurements. This paper is a sequel of two research works [5], [6]. In addition to those previous studies, this paper tests the open-source workflow using high-resolution data for the first time. First, this paper provides an overview of the PS-InSAR technique, highlighting its fundamental concepts. Then, it describes a case study and presents the results. Especially, the comparison is made between two stacks of images with different spatial resolutions, and between GNSS and PS-InSAR outcomes. Finally, the results are discussed.

PERMANENT SCATTERER INTERFEROMETRY SYNTHETIC APERTURE RADAR (PS-INSAR)

Radar satellites radiate electromagnetic waves at various microwave bands toward an area of interest. Some of the signal is reflected back to the sensor, and its phase is influenced by the target-sensor distance, surface topography, and ground displacement along the Line Of Sight (LOS). The phase is also affected by atmospheric pressure, water vapor, and soil moisture [7]. PS-InSAR algorithms aim at obtaining the deformation rate of the target by analyzing radar images acquired over the same area at different times. The phase change among two images which generate the i-th interferogram, $\Delta\varphi_i$, can be described as follows [8].

$$\Delta\varphi_i = \frac{4\pi}{\lambda}\Delta r_{Ti} + \Delta\alpha_i + \Delta n_i + \varepsilon_{topo,i} \quad (1)$$

where Δr_{Ti} is the phase change due to the movement in the LOS direction, $\Delta\alpha_i$ is the atmospheric phase contribution, λ is the radar system wavelength, Δn_i is the decorrelation noise and $\varepsilon_{topo,i}$ is the phase contribution due to possible errors in the Digital Elevation Model (DEM). An essential condition to accomplish the separation of Δr_{Ti} from the other terms in Eq. (1) is to analyze pixels characterized by small decorrelation noise typically related to reflectors where the response to the radar is

dominated by a strong reflecting object and is constant over time (Permanent Scatterer, PS). The first pioneer work based on PS-InSAR was proposed by Ferretti et al. [9]. Another important PS-InSAR contribution was given by Hooper et al. who proposed a novel PS selection method based on the use of phase characteristics. This work originated one of the most widely used PS-InSAR software packages, StaMPS [10]. Nowadays, due to data availability and some freely available SAR services, such as the ESA services and Sentinel 1 images, data for PS-InSAR processing becomes more accessible, and it can be run also by an open-source processing chain [4].

In this study, the SNAP-StaMPS workflow is utilized, according to Figure 1. The SNAP processing includes all the essential steps for preparing the required products to conduct persistent scatterer processing using StaMPS. The SNAP workflow involves the following steps: 1) Optimal master image selection; 2) Product splitting, to ensure consistent sub-swath and burst selection across all images facilitating successful co-registration; 3) Orbital correction using the available precise orbit files; 4) Coregistration using the Back Geocoding operator to align the images accurately; 5) Debursting to merge the adjacent burts in the azimuth direction; 6) Topographic phase removal using SRTM 3 arc-second DEM model; 7) interferogram formation; 8) StaMPS export. The StaMPS processing, starting from interferograms, involves the following steps: 1) Data loading and preparation of the dataset required for the PSs processing; 2) Phase noise estimation for each candidate pixel in every interferogram; 3) Selection of eligible persistent scatterer pixels on the basis of noise characteristics and, PS weeding that is discarding of noisy PS or PS affected by signal contributions from neighboring elements; 4) Phase correction of the wrapped phase for spatially uncorrelated look angle error, and merging of the patches of interest; 5) Phase unwrapping and 6) Exporting displacements. For a more comprehensive understanding of the workflow, refer to [4].

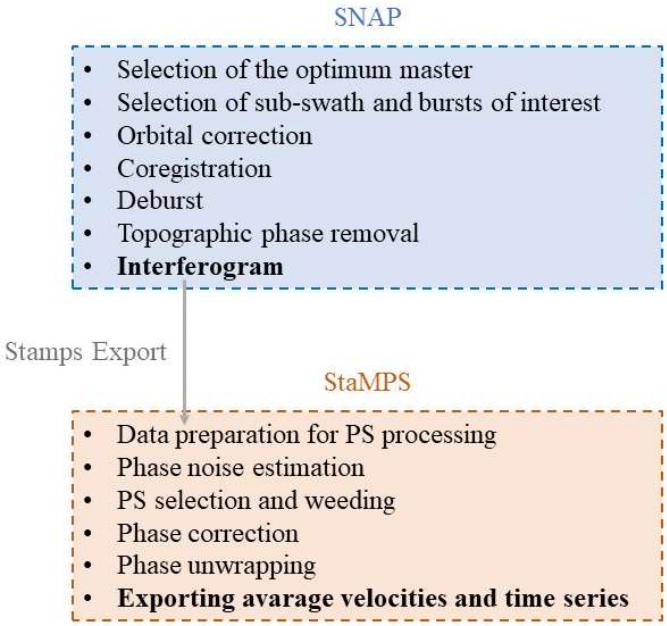

Figure 1: Combined SNAP–StaMPS workflow.

CASE STUDY

The case study is a concrete bridge situated in Isola Dovarese, a municipality of the Cremona province, Italy. The GNSS-based SHM system deployed on the Isola Dovarese Bridge consists of ten receivers mounted on the deck and the piers of the two central spans, see Figure 2 (a). The GNSS monitoring system provides the relative displacements of ten key points of the bridge with respect to the master receiver ID01. The GNSS system provides measurements through the relative static positioning method with planimetric and altimetric accuracy of 0.2 and 0.4 mm, respectively. This study considers data associated with deck-mounted receivers, namely ID04 and ID08 installed on the east side of the bridge and ID05 and ID09 installed on the west side of the bridge. Figure 2 (b) illustrates the relative orientation of the bridge with respect to the North and East directions.

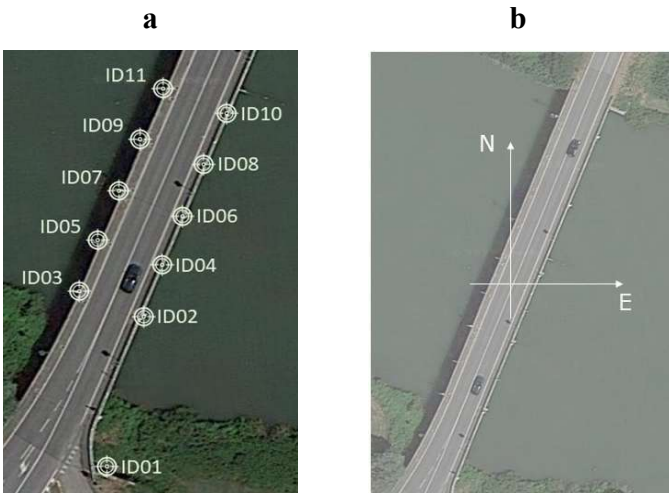

Figure 2. Isola Dovarese Bridge: (a) Planimetric location of GNSS receivers. (b) The orientation of the bridge with respect to the North and East directions.

PS-INSAR RESULTS AND DISCUSSION

In this section, the PS-InSAR results are presented. Two studies are carried out. The first comparison assesses the influence of the geometrical resolution of radar images on PS-InSAR results. The second study compares the PS-InSAR results against in-situ GNSS measurements.

Different radar images

For the first comparison study, the PS-InSAR datasets include two different stacks of radar images. The first stack consists of 55 Sentinel 1 (S1) scenes covering the period from October 2020 to August 2022, acquired in ascending orbit mode and freely provided by the ESA (through the Sentinel-1 satellite mission). These 55 Single Look Complex (SLC) images were acquired through the Interferometric Wide (IW) swath mode with a geometric resolution of approximately 5 m x 20 m. Sentinel 1 satellites are equipped with a C-band radar system featuring a frequency range of 4–8 GHz and a

wavelength of ~ 5.6 cm. The second stack includes 38 Cosmo SkyMed (CSK) data acquired over a period from August 2018 to July 2022. These 38 images are acquired in Strip MAP HIMAGE mode with a geometric resolution of approximately 3 m x 3 m. CSK satellites are equipped with an X-band (9.6 GHz with a wavelength of ~ 3.1 cm). Both stacks of images are processed through the open-source workflow (based on SNAP and STAMPS software) run in a workstation equipped with 128 GB of RAM. Figure 3 (a) and (b) display the PSs obtained by processing 55 S1 and 38 CSK images, respectively. The processing of CSK images reveals a higher number of PSs, particularly in the northern area of the bridge Figure 3 (b).

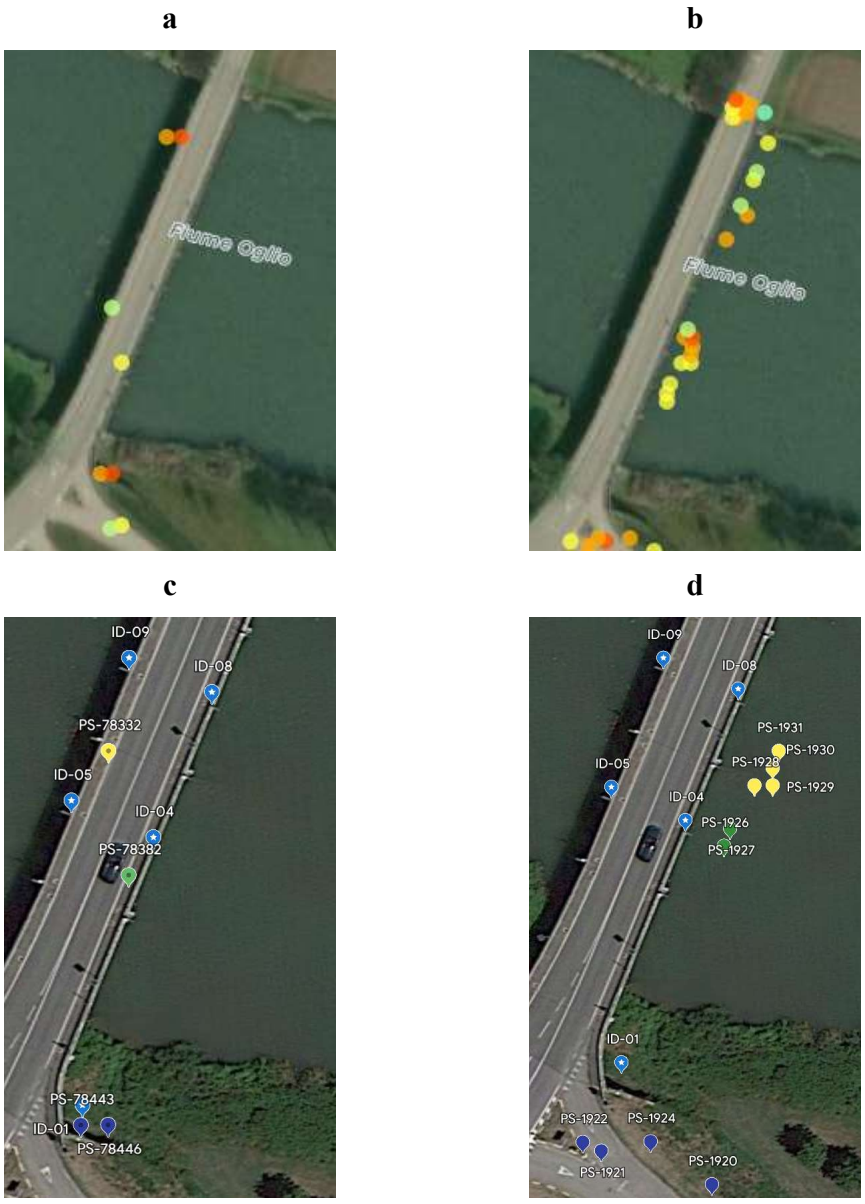

Figure 3. (a) PSs obtained by processing 55 S1 images, (b) PSs obtained by processing 38 CSK images. (c) PSs obtained by processing S1 images on the deck portion monitored by GNSS system, (d) PSs obtained by processing CSK images on the deck portion monitored by GNSS system

The PSs that show a strong correlation in displacement trends and are geometrically close are merged by computing their average displacement, resulting in a reduced total number of PSs. Especially, related to the portion of the bridge which is monitored by the GNSS system, the output of the first PS-InSAR processing S1 images provides two PSs on the deck portion (PS-78332 and PS-78382 in Figure 3 (c)) already monitored by the GNSS system and two PSs in the area of the master GNSS receiver (ID01). In the same area of the bridge, seven PSs were founded by processing CSK images (PS-1926, PS-1927, PS-1928, PS-1929, PS-1930, PS-1931 in Figure 3 (d)). In the area of the master GNSS receiver (ID01) four PSs are available by using CSK images (PS-1920, PS-1921, PS-1922, PS-1924 in Figure 3 (d)).

Displacement magnitude

The second comparison study aims to evaluate the quality of the measurements obtained through PS-InSAR against the in-situ ones retrieved by mean a GNSS monitoring system. To compare zero mean displacement time series, for each dataset, the mean displacement is subtracted. To allow for the comparison, the vertical, d_{up}, and the planimetric component, d_{est}, of the PS-InSAR LOS displacement are estimated as follows:

$$d_{up} \sim \cos(\theta)\, d_{los} \qquad (2)$$

$$d_{est} \sim \sin(\theta)\, d_{los} \qquad (3)$$

where θ is the average value of the incidence angle between the LOS displacement d_{los} and the vertical direction. The comparison between PS-InSAR output and in situ GNSS measurements is based on the relative displacements with respect to the GNSS master receiver ID01. The GNSS system provides the relative (both vertical and horizontal) displacement of the slave receivers ID04, ID05, ID08, and ID09 with respect to the master receiver ID01. In the processes, the PSs that show a strong correlation in displacement trends and are geometrically close are merged by computing their average displacement. The PS-InSAR relative displacement time histories are obtained by subtracting the PSs absolute displacement from the displacement of PSs near the master receiver ID01: for instance, in the case of Sentinel 1 outputs (Figure 3 (a)), the relative displacements (both vertical and horizontal) of PSs 78332 and 78382 are derived by subtracting their absolute displacements from the average displacement of PSs 78443 and 78446. Similarly, for PSs derived from processing CSK images (Figure 3 (b)), the relative displacements for comparison with GNSS receivers ID04 and ID08 are obtained using similar calculations. Especially, the PS-CSK-1 displacement time history is obtained by subtracting the average absolute displacement of PSs 1926 and 1927 from the average absolute displacement of PSs 1920, 1921, 1922, and 1924. Similarly, the PS-CSK-2 displacement time history is obtained by subtracting the average absolute displacements of PSs 1928-1931 from the average absolute displacement of PSs 1920, 1921, 1922, and 1924. The vertical and horizontal retrieved by using Sentinel 1 images are presented in Figures 4 (a) and (b), respectively. Figure 4 (c) and (d) present a comparison between the relative displacement of PSs resulting from Cosmo Sky-Med images processing.

The comparison between PS-InSAR measurements obtained from processing Sentinel 1 and Cosmo Sky-Med images reveals interesting new results with respect to the

previous works [5], [6]. Figure 4 (a) and (b) indicate that the PS-InSAR measurements derived from Sentinel 1 images surpass the vertical and planimetric displacement estimated by GNSS, in accordance with the previous findings [6]. However, Figure 4 (c) and (d) highlight a significant improvement in measurement precision when processing Cosmo Sky-Med images. The PS-InSAR measurements achieved using Cosmo Sky-Med images lead to a more accurate estimation of the amplitude displacement, especially in the transversal direction as depicted in Figure 4 (d). These new findings demonstrate that Cosmo Sky-Med images provide more precise magnitude measurements, enhancing the reliability of the results.

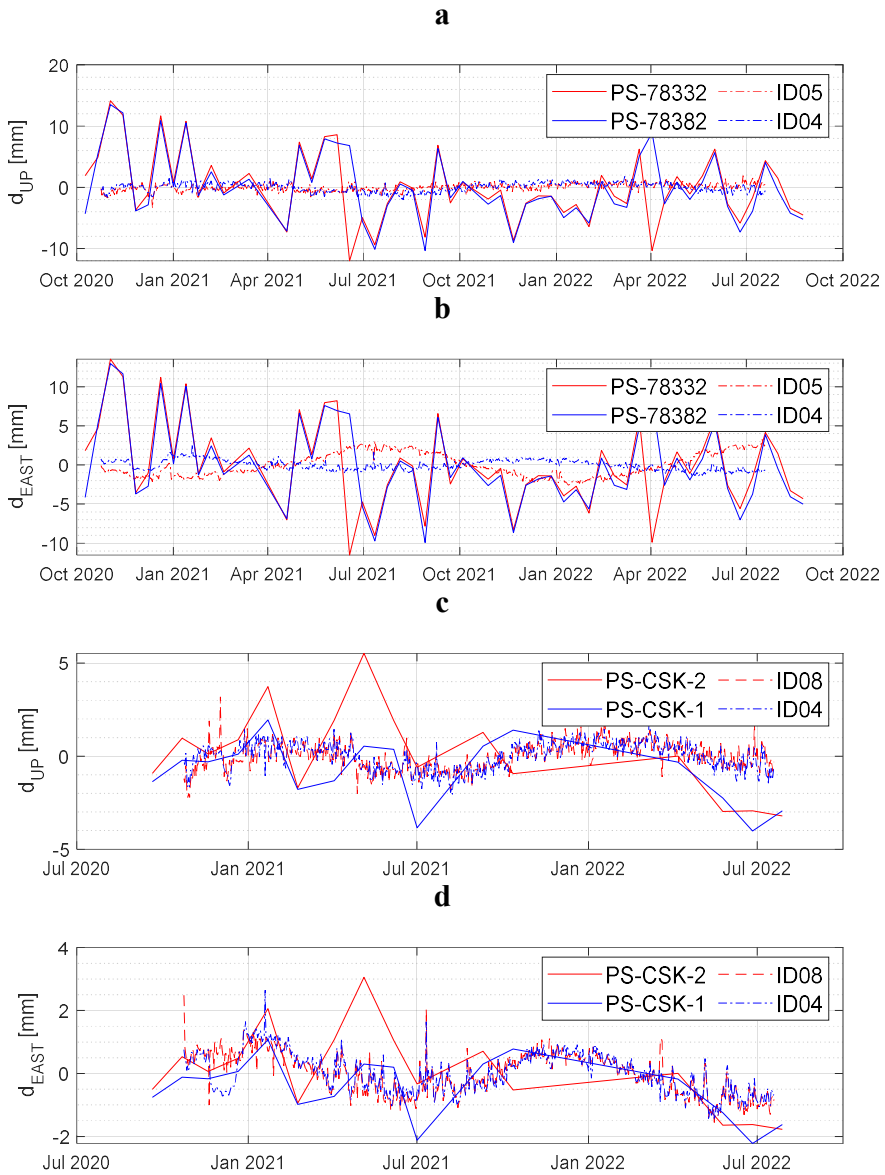

Figure 4. Relative displacement of the deck: (a) vertical displacement (Sentinel 1 dataset); (b) horizontal displacement (Sentinel 1 dataset). (b) vertical displacement (CSK dataset); (b) horizontal displacement (CSK dataset).

CONCLUSIONS

In this paper, the PS-InSAR technique is implemented using open-access software to investigate the structural behavior of a concrete riverine bridge in Northern Italy, on which a GNSS monitoring system is installed. The displacements of the bridge are mainly influenced by environmental effects. The numerosity of the PSs found on the bridge is influenced by the type of radar images processed. Especially, the high spatial resolution images (acquired through Cosmo SkyMed satellite mission) provide more PSs on the structure with respect to the low spatial resolution images (acquired through Sentinel 1 mission). The magnitude of the displacement obtained through a PS-InSAR application that uses Sentinel 1 images is not comparable to those obtained through GNSS measurement. By processing CSK images, the estimation of the displacement magnitude improves, especially in the horizontal direction. A more accurate estimation of vertical and horizontal displacement can be attained by combining data from the ascending and the descending orbits.

REFERENCES

1. J. T. Salzer, P. Milillo, N. Varley, D. Perissin, M. Pantaleo, and T. R. Walter, "Evaluating links between deformation, topography and surface temperature at volcanic domes: Results from a multi-sensor study at Volcán de Colima, Mexico," *Earth Planet Sci Lett*, vol. 479, pp. 354–365, Dec. 2017, doi: 10.1016/j.epsl.2017.09.027.
2. P. Milillo *et al.*, "Heterogeneous retreat and ice melt of Thwaites Glacier, West Antarctica," *Sci Adv*, vol. 5, no. 1, Jan. 2019, doi: 10.1126/sciadv.aau3433.
3. P. Milillo, G. Giardina, D. Perissin, G. Milillo, A. Coletta, and C. Terranova, "Pre-Collapse Space Geodetic Observations of Critical Infrastructure: The Morandi Bridge, Genoa, Italy," *Remote Sens (Basel)*, vol. 11, no. 12, p. 1403, Jun. 2019, doi: 10.3390/rs11121403.
4. F. Mancini, F. Grassi, and N. Cenni, "A Workflow Based on SNAP–StaMPS Open-Source Tools and GNSS Data for PSI-Based Ground Deformation Using Dual-Orbit Sentinel-1 Data: Accuracy Assessment with Error Propagation Analysis," *Remote Sens (Basel)*, vol. 13, no. 4, p. 753, Feb. 2021, doi: 10.3390/rs13040753.
5. O. Lasri, P. F. Giordano, M. P. Limongelli, and M. Previtali, "Remote monitoring of a concrete bridge: validation of SAR satellite monitoring results using GNSS data," in *2nd Conference of the European Association on Quality Control of Bridges and Structures (EUROSTRUCT)*, 2023.
6. O. Lasri, P. F. Giordano, M. Previtali, and M. P. Limongelli, "Remote monitoring of a concrete bridge through InSAR and GNSS measurements," in *Eighth International Symposium on Life-Cycle Civil Engineering (IALCCE)*, 2023.
7. D. Cusson, K. Trischuk, D. Hébert, G. Hewus, M. Gara, and P. Ghuman, "Satellite-Based InSAR Monitoring of Highway Bridges: Validation Case Study on the North Channel Bridge in Ontario, Canada," *Transportation Research Record: Journal of the Transportation Research Board*, vol. 2672, no. 45, pp. 76–86, Dec. 2018, doi: 10.1177/0361198118795013.
8. A. Ferretti, C. Prati, and F. Rocca, "Permanent scatterers in SAR interferometry," *IEEE Transactions on Geoscience and Remote Sensing*, vol. 39, no. 1, pp. 8–20, 2001, doi: 10.1109/36.898661.
9. A. Ferretti, C. Prati, and F. Rocca, "Permanent scatterers in SAR interferometry," *IEEE Transactions on Geoscience and Remote Sensing*, 2001, doi: 10.1109/36.898661.
10. A. Hooper, "A multi-temporal InSAR method incorporating both persistent scatterer and small baseline approaches," *Geophys Res Lett*, vol. 35, no. 16, p. L16302, Aug. 2008, doi: 10.1029/2008GL034654.